

# The transient dynamics of dilation waves in granular phase transitions during silo discharge

L. A. Fullard<sup>1</sup> · C. E. Davies<sup>2</sup> · G. Lube<sup>3</sup> · A. C. Neather<sup>3</sup> · E. C. P. Breard<sup>3</sup> · B. J. Shepherd<sup>4</sup>

Received: 5 April 2016 / Published online: 21 November 2016  
© Springer-Verlag Berlin Heidelberg 2016

**Abstract** Granular material has the unique ability to transition between solid and liquid-like phases, but quantitative observations of the dynamics involved in this process remain rare. We hypothesize that granular packing of the solid phase has a leading control on this transition. To test this, we visualize the flow transitions that occur during discharge from a grain-filled silo. X-ray fluoroscopy and high-speed video analysis are used to detect and characterize the kinematics of dilation waves that trigger the phase transitions. Wave velocities are shown to vary by an order of magnitude with strong dependence on the packing density of the initially static bed. The speed of dilation waves exceeds any granular flow velocity in the system, and a simple model based upon conservation of mass is presented to describe this phenomenon. Our results have major implications for the quantitative description and prediction of granular system behaviour in natural and industrial applications, particularly with regards to the onset of avalanche motion and the handling of powders and grains.

**Keywords** Granular material · Silo · Dilation

## 1 Introduction

The study of dense granular flow is a necessary endeavour. In the U.S., industrial processing of powder and grains is worth trillions of dollars annually [28], yet the physics of granular matter and granular flow in particular underlying these processes are poorly understood compared to the flow of most fluids.

Of interest in many different areas of science and industry are the processes occurring during transition from a static granular bed to a flowing granular material. These granular phase transitions are common in natural processes (e.g., erosion and deposition in geophysical mass flows, the initial motion of a snow avalanche, processes of earth movement during earthquakes [10, 19, 20]) and man-made situations (e.g., the motion of people groups and traffic flow [38], and in the handling of bulk-solids industry [24]). Still, a complete explanation or an accepted quantitative theory for these processes is lacking [1]. It is known that a granular material must first dilate before flow will initiate [4–6, 23, 24]. We hypothesize that the dynamics and kinematics of this transition are dependent on the initial solids bulk density; in other words a loosely compacted static bed will transition more easily into a flowing state than a more compacted bed. The triggering time for an underwater avalanche was found to increase as the solids fraction increased in experiments by previous authors [25]. The self-filtration phenomenon [37] in concentrated suspensions appears to share some similarities with the initiation of flow in a silo. It has been noted [11] that concentrated suspensions which are driven through a contraction by a pressure gradient, and which have a high solids fraction, undergo repeated jamming and rapid fracture (unjamming) events which originate near the exit orifice. Particle rearrangement (dilation) allowed the suspended particles to expand and flow with the consequence that liquid was

✉ L. A. Fullard  
L.Fullard@Massey.ac.nz

<sup>1</sup> Institute of Fundamental Sciences, Massey University, Palmerston North, New Zealand

<sup>2</sup> School of Engineering and Advanced Technology, Massey University, Palmerston North, New Zealand

<sup>3</sup> Volcanic Risk Solutions, Massey University, Palmerston North, New Zealand

<sup>4</sup> Radiography Department, Palmerston North hospital, Palmerston North, New Zealand

drawn into the volume abandoned by the particles (Reynolds dilation phenomena). Shear-induced dilation was also shown to reduce fluid pressure in self-filtration experiments with concentrated suspensions [18]. Kulkarni et al. [18] developed a simple mathematical model which related the shear-rate, the particle pressure, and the solids volume fraction in a channel to the solids fraction after the suspension had passed through a contraction. In the context of bunker discharge, (so-called) dilation waves are envisaged to control the occurrence of granular phase transitions and, importantly, the magnitude of resulting flow phenomena such as hopper mass flow rates [34]. However, systematic investigations to explain the origin and nature of granular dilation waves are still missing. Some mathematical models have attempted to incorporate dilation phenomena in the description of flow [2, 16, 33, 36], yet experimental measurements to validate models are few [7, 21]. Using an X-ray subtraction technique, Baxter et al. [3] were the first to directly observe that during granular solid-liquid-like transition in a hopper, a dilation wave develops and rapidly travels vertically away from the hopper opening. Many aspects of this mechanism, however, remain unknown, including the kinematic behaviour of these waves, and their dependence on the characteristics of the granular material (e.g., the initial packing, grain-size, sorting, etc.). Henceforth, we refer to the transition from a stationary packed bed of particles to a flowing regime as a solid-liquid-like transition. In this study, we use a flat bottomed quasi-2D silo as an analogy to investigate the role of dilation waves in controlling granular solid-liquid-like transitions. At the beginning of this study, we hypothesize that flow from the silo will only be steady when the dilation wave has fully propagated through the system.

## 2 Experimental method

To quantify the transient dilation phenomena, we visualised and tracked the dilation wave in a flat-bottomed silo, generated upon flow initiation using X-ray fluoroscopy (Philips Allura Clarity fluoroscopy machine) and a particle image velocimetry (PIV) image analysis method. The experiments were repeated using three filling methods, each of which produced a different initial solids fraction. A custom built flat-bottomed silo was constructed from perspex. A labelled figure of the set-up is shown in Fig. 1. The upper feed hopper was filled from above with granular material which could flow into the test area, the flat-bottomed silo. Separating these two was the upper slider which could be closed to terminate the flow. This slider remained open during the experiment so that the test section of the silo was always filled with the granular material. The test silo has dimensions 200 mm width, 350 mm height, and 15 mm depth, so chosen to fit the field of view of the X-ray fluoroscopy machine. Separating

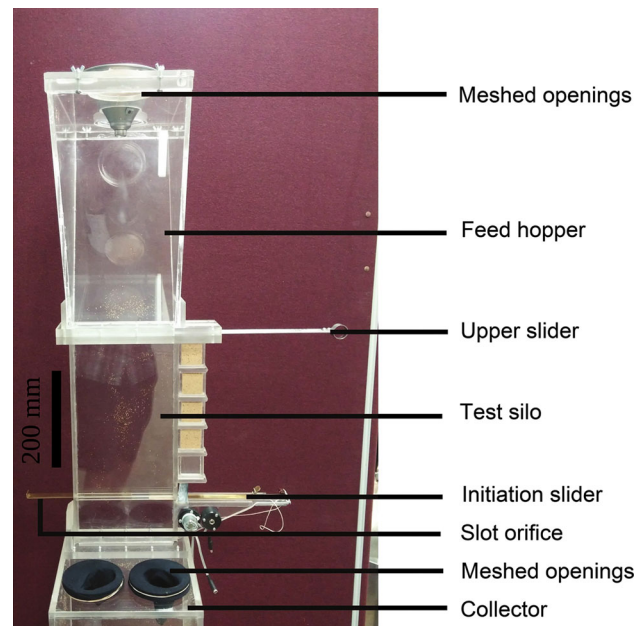


**Fig. 1** The labelled experimental apparatus used for this study

the test silo from the collector are two brass sliders. The upper slider contains an 8 mm slot orifice which spanned the depth of the silo. The lower slider is the initiation mechanism and is attached to an electric motor so that the flow could be initiated remotely to avoid exposure to X-ray radiation and to ensure flow was initiated in a consistent way. On the top of the feed hopper and on the collector below the silo were two vents covered with a fine mesh to ensure that the pressure is atmospheric above and below the silo. The granular material used was amaranth, *Amaranthus*, which was free flowing, ovoid in shape, had an average major diameter of 1 mm, and had a true particle density of  $1310 \pm 10 \text{ kg/m}^3$ , measured using a pycnometer (Ultrapycnometer 1000, Quantachrome instruments).

To investigate the dependence of granular transitions on initial packing during discharge from a silo, the granular material was loaded using three different methods which produced: (1) a high density packing, (2) a medium density packing, and (3) a low density packing. The resulting density of packing is summarised in Table 1. For each experimental run the amaranth seeds were loaded into the upper feed hopper using one of the following three loading methods:

1. A *low density fill* with the upper slider closed, the grain was poured through a funnel and loaded up the upper hopper. Once the upper feed hopper was filled to a satisfactory level, the upper slider was opened and the test silo was filled by the falling material.

2. A *medium density fill* the filling method (1) for the low density fill was first performed, followed by 60 s of tapping on the side walls of the hopper and silo to consolidate the sample somewhat.

**Table 1** Bulk density and solids fraction for the three filling methods

	Bulk density (kg/m <sup>3</sup> )	Solids fraction ( . )
High density	870 ± 10	0.66 ± 0.01
Medium density	830 ± 10	0.63 ± 0.01
Low density	800 ± 10	0.61 ± 0.01

3. A *high density fill* with the upper slider open, the grain was poured through a funnel and loaded up the test silo directly. Upon filling, the grains first bounced off the upper feed hopper walls, then fell into the test silo. This was found to produce an even repeatable fill. Enough material was loaded so that the feed hopper never fell below a certain level to ensure consistent flow.

The solids fractions for the three filling methods differed significantly. The low density fill undergoes a dilation process when the material is transferred from the upper feed hopper to the silo, hence, it has a lower bulk density than does the high density fill, which is loaded directly into the test section and has not yet undergone a dilation process post-packing. The medium density fill has a higher solids fraction than the low density fill due to a tapping process post-loading. We note that the material in the upper feed hopper will be at the initial fill density (the high density case) for every experiment. For the medium and low density fills the material initially dilates as it falls from the upper hopper to the test section, but the remaining material in the upper hopper does not fall, and hence, does not dilate. However, we are primarily concerned in measuring the dilation wave velocity in the test section, and the upper hopper acts only to feed material into the test section, and does not affect the measurements. In fact, for the material to transit from the upper hopper to the test section the dilation wave must pass through the upper hopper. Although we could not measure this, we expect that material entering the test section from the upper hopper after flow initiation will be at constant density.

To quantify the dilation processes occurring during silo discharge we conducted two types of experiments. The silo was set up in the Palmerston North (New Zealand) hospital radiography department. A Philips Allura Clarity X-ray fluoroscopy machine was used to scan the granular system to visualise density changes as flow was initiated. The scanning rate was 15 frames per second (FPS) and 50 s of imaging was performed post flow initiation. Resulting digital image files were analysed using an image subtraction technique. An initial mask image was taken of the loaded system prior to flow initiation, a Gaussian noise filter was applied to each frame of the flowing system, then the initial mask was subtracted from each image (for comparison with the initial packing). The flow patterns in the system were found to be repeatable as long as care was taken in the filling process. We were

able to visualise density changes, but, due to internal image processing software in the Philips machine, we were unable to quantify the density itself. The experiments were repeated with images being obtained using a high speed digital camera at a frame rate of 340 FPS (Basler acA 2000–340 km). The resulting digital image files were passed through the PIV software PIVlab to obtain two-dimensional velocity fields of particles in contact with the hopper front pane [31, 32]. The amaranth grains were found to have reasonably low friction, and were able to slide along the perspex relatively freely. There will be some friction between these surfaces, and the wall velocity may not be completely indicative of the flow in the bulk. In the literature [27], the angle of internal friction for amaranth has been given as 28°, and the angle of wall friction with perspex, 25°, which suggest that the frictional properties at the wall and in the bulk should be similar. In some sample tests, we approximate the reduction of velocity at the wall due to friction to be between 2 and 5% that of the bulk. The authors are working on methods to obtain velocity field measurements in 3D silos.

## 3 Results

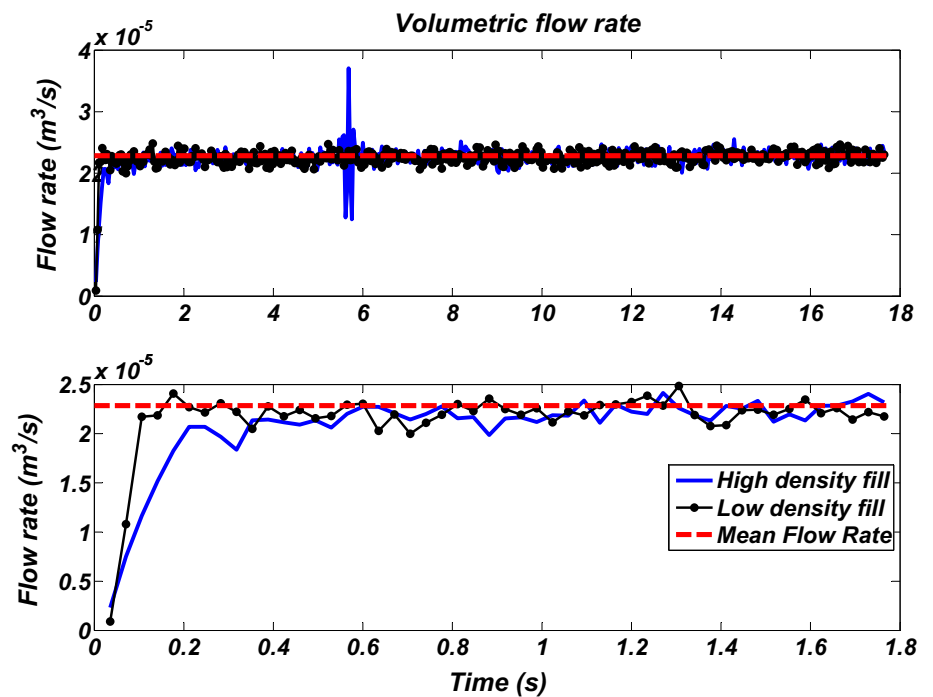
### 3.1 Volumetric flow rate

The velocity fields measured using PIV were numerically integrated using a Matlab script to obtain an indirect measurement of the volumetric flow rate,  $Q$ , by the equation

$$Q = T \int_{-w/2}^{w/2} v dx,$$

where  $T$  is the depth of the silo (15 mm),  $w$  is the width of the silo,  $v$  is the vertical component of velocity, and  $x$  is understood to be the horizontal coordinate. We assume that the velocity is approximately constant across the depth of the silo. The flow rate was independent of the height where the integration slice was taken above the orifice. To minimise noise we took an average over a range of heights in the test section. Figure 2 displays the volumetric flow rate as a function of time for the low and high density fills. In each experiment, an initial phase of unsteady discharge (with the volumetric flow rate strongly increasing with time) occurred before flow rates started to oscillate close to the long term mean flow rate for the remaining duration of the experiment. The duration of this initial transient volumetric flow varied somewhat for the three cases of different initial packing and lasts  $\approx 0.1$  s for the low density fill,  $\approx 0.35$  s for the medium density fill, and  $\approx 0.4$  s for the high density fill. At the flow rates reported, the transient in the discharge rate accounts for  $<10$  g of material (i.e.  $<1\%$  of the hopper fill). As will become evident, the transient

**Fig. 2** Calculated volumetric flow rate as a function of time for the high and low density fills at long times (*upper*) and soon after flow initiation (*lower*)



in the volumetric flow rate is significantly shorter than the development time of the dilation wave associated with the progressive solid-liquid-like transitions of the granular material.

### 3.2 Flow regimes in the silo

During silo drainage it is visually apparent that the flow behaviour is location dependent; stagnant at/near the side walls, slow and plug like far from the orifice, and rapid close to the orifice. The Bagnold number [13],  $B_n$  separates a macro-viscous regime for  $B_n < 40$ , from a transitional regime for  $40 < B_n < 450$ , and a grain inertia regime,  $B_n > 450$ .

$$B_n = \frac{\rho_p d^2 \lambda^{0.5} \dot{\gamma}}{\mu}$$

where  $\rho_p = 1310 \text{ kg/m}^2$ ,  $d = 1 \text{ mm}$  are the particle density and diameter,  $\mu = 2.0 \times 10^{-5} \text{ Pa s}$  is the dynamic viscosity of air,  $\dot{\gamma}$  is the shear rate (which can be measured using the PIV data), and, with  $\phi$ ,  $\phi_c$  (the solids fraction and maximum possible solids fraction),  $\lambda$  is given by

$$\lambda = \left( (\phi_c / \phi)^{1/3} - 1 \right)^{-1}$$

Although  $\phi$  and  $\phi_c$  are not known a priori, from Table 1  $\phi \leq 0.61$ ,  $\phi_c \geq 0.66$ . We therefore use the values  $\phi = 0.61$  and  $\phi = 0.66$  to obtain the largest possible  $\lambda$  value. With this and the shear rate calculated using the velocity fields

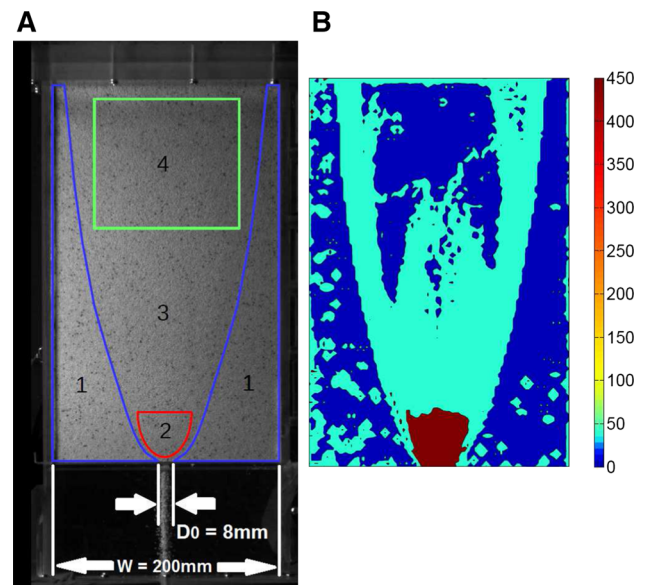


**Fig. 3** **a** An annotated frame of the high speed video. The different regions are labelled based upon the value of the Bagnold number. **b** The spatial distribution of the Bagnold number. Colour contours are *blue* for  $B_n < 40$ , *red* for  $B_n > 450$  and *cyan* between those two values (colour figure online)

generated from the PIV algorithm we calculate the Bagnold number at steady flow in the silo. One high speed image is displayed in Fig. 3a. The different labelled regions pertain to 1. a stagnant zone (by visual inspection), 2. a grain-inertia regime near the orifice, 3. an intermediate regime, and 4. a flowing macro-viscous regime. In zone 4. it was noted that the granular material did not shear (plug flow). Zones 2.–

4. were determined based upon Fig. 3b, where the Bagnold number has been plotted in the flow domain. The blue regions indicate  $B_n < 40$ , the red region  $B_n > 450$ , and the cyan region  $40 < B_n < 450$ .

$B_n$ , and hence the regime zones, were independent of the initial solids fraction as the analysis was performed when the flow was steady. We show in the next section that the transition to steady flow is dependent on the initial packing, but not the steady flow itself.

### 3.3 Visualisation of density and flow

Figure 4a is a visual comparison of the images generated by the X-ray system and the PIV analysis for the high density fill. In both image sets a developing wave is seen to propagate from the orifice opening to the upper end of the test silo. The lighter areas of the X-ray images show a reduction in density associated with the position of the front of the dilation wave. The position of the dilation wave(s) over

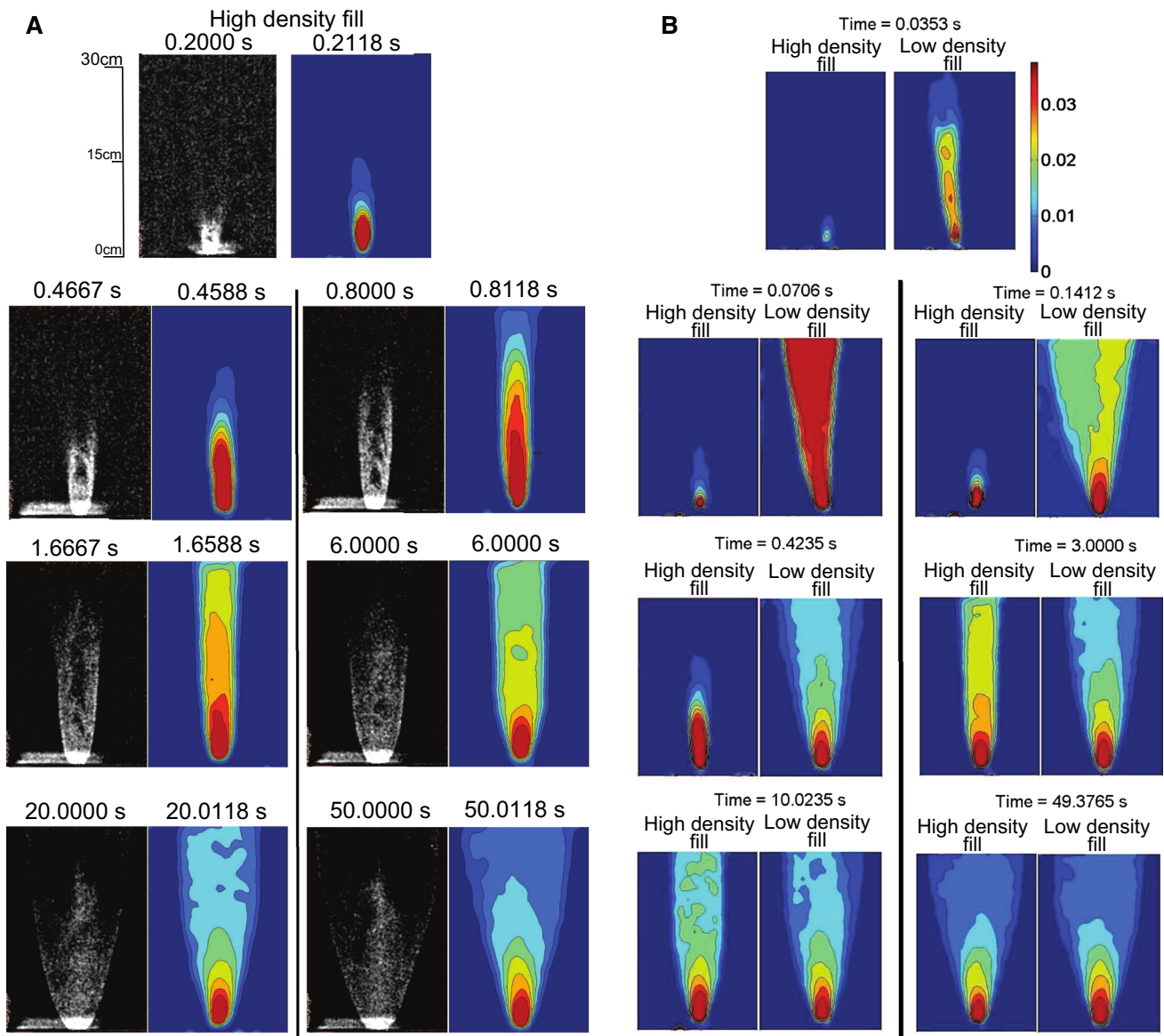


**Fig. 4** **a** Comparison of the processed X-ray (black and white, left) and PIV images (colour, right) for the high density fill. The images are given at similar times after flow initiation but are not exactly the same time due to the difference in FPS rates of the experiments. **b** Compari-

son of PIV images of the high and low density fills. The colours in the PIV images represent the magnitude of velocity (m/s), and are defined in the legend (colour figure online)

time depicted with the X-ray technique coincides well with the spatial and temporal pattern of the waves derived from the PIV analysis. The system must first dilate for flow to begin. It was observed that the flowing zone took about 40 s to reach a steady width, significantly longer than the time taken for a quasi-steady flow rate to develop. After this time the system has a steady flow structure, with a quasi-steady velocity field. For the X-ray images of the low density fill (not shown here) no density wave was visible. The change in bulk density was too small to be noticed using this experimental set-up. The low density fill undergoes a packing change during the filling process, hence the solids fraction change upon discharge is small. Figure 4b is a comparison of the velocity fields during the development of the dilation front for the high and low density fills. During the initial dilation, the wave propagates rapidly from the opening orifice upwards as a thin plug. The granular flow velocities in this region are initially of the same order as the flow velocity near the orifice ( $\approx 0.04\text{--}0.06\text{ m/s}$ ) but reduce as the flowing region spreads horizontally. This high basal velocity is necessary to maintain a constant flow rate while the flowing (liquid-like) region is thin. As the width of the flowing region increases with time, the velocity required to maintain a constant flow rate is reduced. The vertical component of velocity of the travelling wave is high in the case of the (already diluted) low density fill, taking  $<0.07\text{ s}$  for particles at the top of the silo to begin to flow. The wave front for high density fill takes approximately  $0.7\text{ s}$ , hence is travelling more than an order of magnitude more slowly than the low density fill dilation wave. In the low density fill experiment, the propagating wave occupies a significantly larger area at similar times when compared to the high density fill; i.e. it is more efficient to initiate flow across a wide region within the hopper. The high density fill packing must first dilate which results in slower wave speed. Of note is that the two fillings appear to reach the same equilibrium (i.e. after an initial transient, both fills had a similar quasi-static velocity field) as seen in the last image in the sequence. The low density fill reaches this equilibrium is a slightly shorter time. Not displayed here are the images for the medium density fill. The results for this case were similar to the high density fill, suggesting that the consolidation step caused a change in packing, a higher solids fraction, and hence, a larger level of dilation was needed to initiate flow than for the low density fill case. We have also examined the restart flow for the high density fill case. The silo was loaded with the high density fill method and then discharged for  $60\text{ s}$ . The flow was then stopped using the initiation slider and restarted again to see how the dilation wave would develop. The development of the dilation wave for the restart was now comparable with the low density fill case, consistent with the system having already dilated and having little need for further dilation upon restart.

### 3.4 Dilation wave velocity

To measure the dilation wave speed the PIV images were input into a user-written Matlab script. The script took every  $n$ th image and found the vertical position furthest from the orifice where the vertical-component of the velocity exceeded some non-zero threshold. Since PIV generates some noise on even stagnant material, the threshold was chosen to exceed the noise in the PIV analysis. The user was then prompted to click on the left and then the right sides of the flowing region to measure the approximate width of the flowing zone. The number of images (every  $n$ th) was necessarily lower for the faster process, the low density fill. Figure 5 show these results. In the left graph the vertical position of the front of the dilation wave was tracked as a function of time. For each of the three filling methods the relationship was approximately linear and the slopes of the plots indicate the vertical dilation propagation speed. As observed visually in Fig. 5, the low density fill dilation wave velocity was an order of magnitude faster than the other two cases, while the speed of the medium density fill dilation wave was double that of the high density fill. It was noted that, even in the densest packing, the high density fill (the system with the slowest developing dilation wave), the wave velocity was always greater (and in the opposite direction) than any particle velocity in the system. The development of the dilation wave is very sensitive to the initial solids fraction after filling. The right hand graph of Fig. 5 shows the development of the width of the flowing zone. For all three cases the wave takes  $>30\text{ s}$  to reach a steady width, significantly longer than the time for the vertical wave to propagate the same distance. As previously noted, a consequence of this relatively slow widening of the flowing zone is initially rapid particle velocities (when the flowing zone is narrow) which decrease as the flowing zone width increases. This ensures that the flow rate during the widening of the flow zone is constant (the transient on the flow rate is  $<<1\text{ s}$ , see Sect. 3.1). We suspect that these observations have important implications for experimental and modelling studies of granular material, since many studies neglect the transient development of flow. Our results indicate that there is a significant time necessary for a system to be considered in a steady state, and experimentalists would be wise to account for this when developing methodology, particularly in measurements of residence time distribution and mixing indices.

### 3.5 Mathematical model of dilation

We here modify the dilation propagation model found in [35] to predict the velocity of the dilation wave for comparison to the results in Fig. 5. Consider a bed of tightly packed particles as shown above the black line in Fig. 6. When these particles are exposed to a gravitational force the bottom layer

**Fig. 5** For the three filling methods: *left* position and velocity of the vertical edge of the dilation front as a function of time. *Right* width of the dilation wave as a function of time

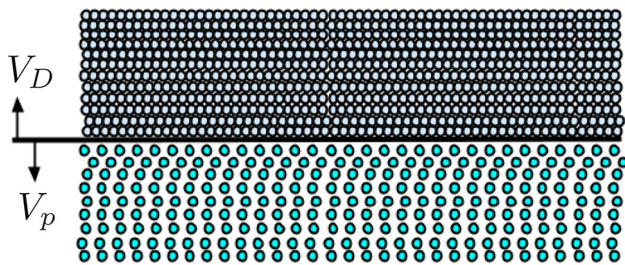
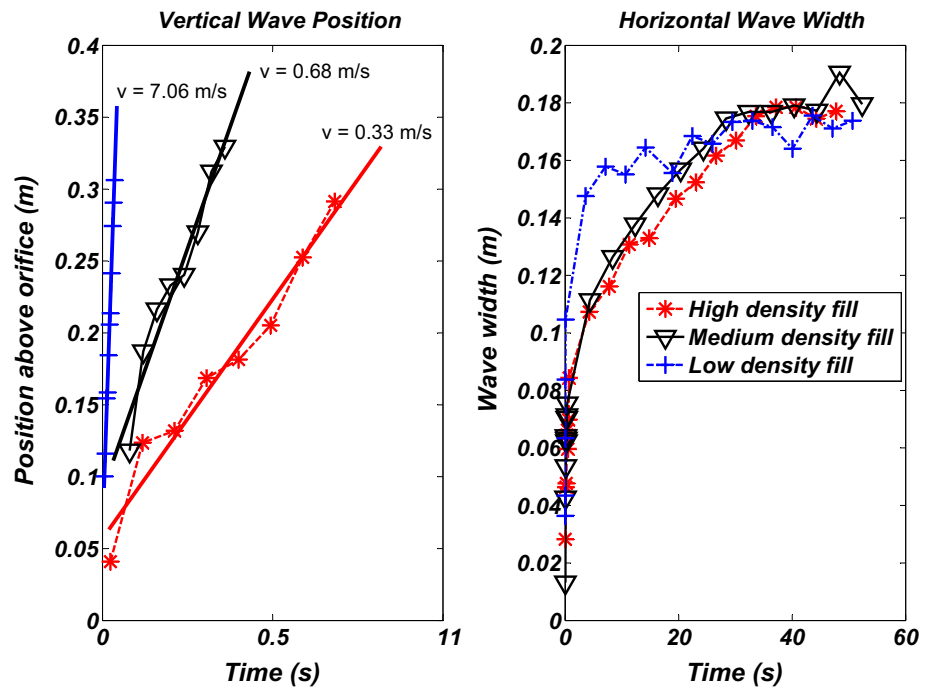


**Fig. 6** A dilation wave with speed  $V_D$  propagates upwards (in the opposite direction of flow) into a dense granular bed. Below the dilation wave the particles fall with velocity  $V_p$

of the packed begins to flow with velocity  $V_p$  downwards (below the black line). As each individual horizontal layer begins to flow, the average density at the bottom of the bed decreases (dilates) and the front of dilation moves vertically with velocity  $V_D$ . Conservation of mass in the system allows us to write an equation for mass flow per unit area:

$$-Jdt = \Delta\rho dS_D$$

where  $J = \rho V_p$  is the mass flux of grains in the lower flowing zone,  $\rho$  is the bulk density in the dilated flowing zone,  $\Delta\rho = \rho_0 - \rho$  is the change in bulk density,  $\rho_0$  is the bulk density in the packed bed above the flowing zone, and  $dS_D$  is the distance which the dilation front moves vertically in time  $dt$  due to the lower layer of particles breaking away from the packed bed. We can rearrange this equation to find the dilation front velocity:

$$\frac{dS_D}{dt} = V_D = -\frac{\rho}{\Delta\rho} V_p$$

For an orifice of diameter  $D_0$ , the characteristic velocity at the orifice is given by

$$V_o \approx -\sqrt{gD_0}$$

where  $g$  is the acceleration due to gravity. At some distance above the orifice, the dilation wave has width  $W$ . By conservation of mass, the flowing zone has characteristic velocity

$$V_p \approx -\sqrt{gD_0} (D_0/W) = -\sqrt{g} D_0^{3/2} / W.$$

Hence, the velocity of the dilation wave is given by

$$V_D \approx \frac{\rho}{\Delta\rho} \frac{\sqrt{g} D_0^{3/2}}{W}.$$

Although the flowing zone width  $W$  varies in time, for simplicity we approximate an average value. From our experimental measurements, we approximate the width of the developing dilation zone  $W \approx 70$  mm. We assume that the three packings will reach an identical flowing density after the passing of the dilation wave. We have no measured value of  $\Delta\rho$  so we use the low density fill to approximate this value from the measured wave speed, then compare the results to the other two fills. This calculation gave  $\Delta\rho \approx 3.6$  kg/m<sup>3</sup>. We can approximate the velocity of the dilation wave and compare to results in Fig. 4. This comparison is shown in Table 2.

**Table 2** Vertical dilation wave speed as measured experimentally and predicted using the mathematical model

	Predicted (m/s)	Measured (m/s)
High density ( $870 \pm 10 \text{ kg/m}^3$ )	$0.38 \pm 0.06$	0.33
Medium density ( $830 \pm 10 \text{ kg/m}^3$ )	$0.79 \pm 0.32$	0.68
Low density ( $800 \pm 10 \text{ kg/m}^3$ )	–	7.06

The confidence intervals widen as  $\Delta\rho$  becomes smaller (initial packing density closer to the flowing density). For this reason the interval is wider for the medium density case than for the high density case. Nevertheless, the conceptual model is shown to capture the order of magnitude of the vertical speed of the dilation wave.

### 3.6 Dilation wave structure

Finally, we describe the structure of the dilation waves at early times as observed in the X-ray images. Figure 7 shows the observed x-ray results for the high density fill case at four times during the development of the dilation wave. We note that we did not observe any density change for the low density fill case. The zones of reduced density occur in three main regions: (i) a fast flowing region of large dilation immediately above the orifice, (ii) an internal region where the flow is developing, and (iii) thin linear regions which encircle the flowing region. This third region propagates upwards as symmetric bands after flow initiation and separates flowing from stationary material, and can be thought of as a shear plane. At certain times in the flow, these thin bands converge together to form an arc shape, noted in the figure by arrows. Once these

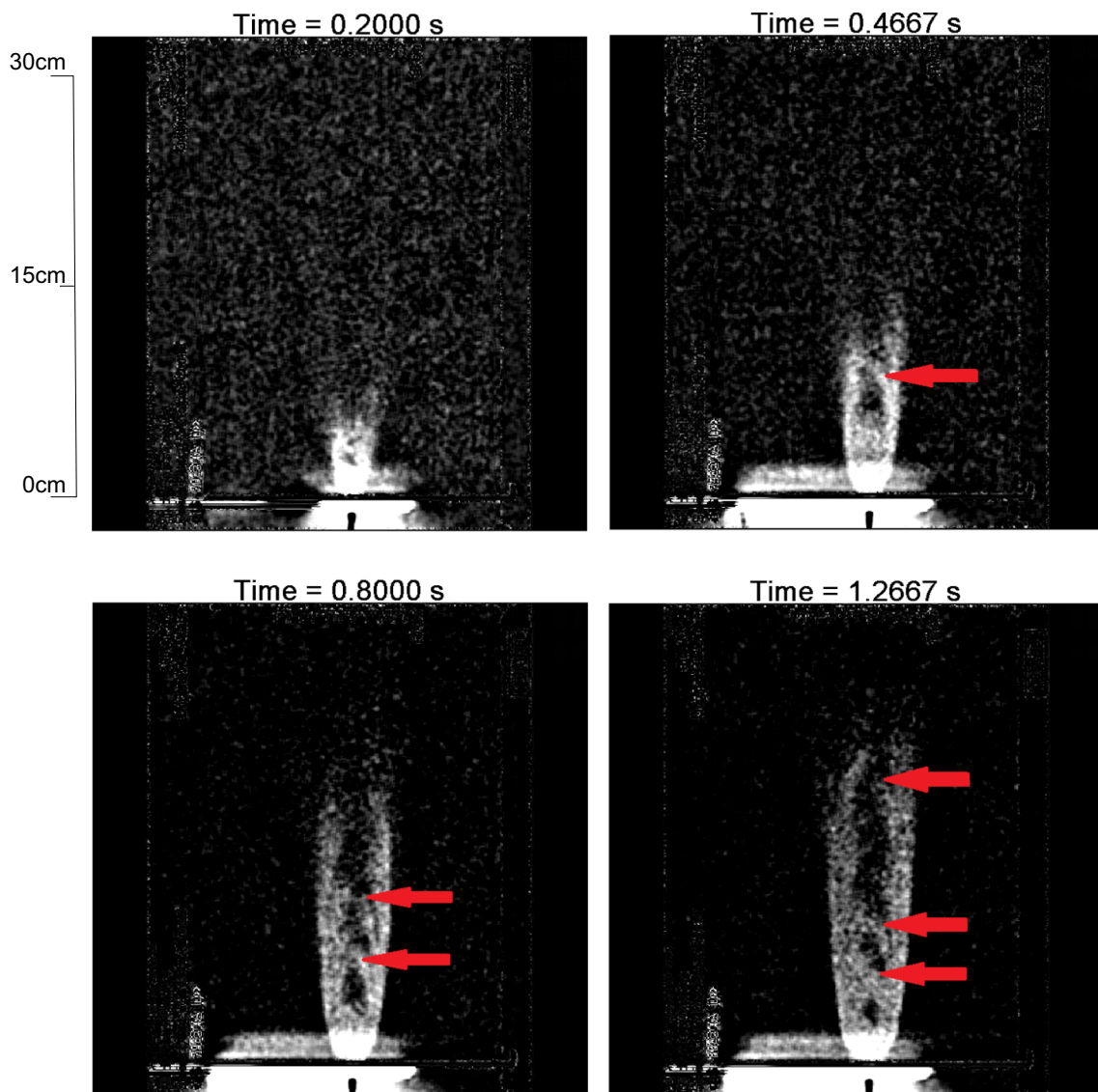


**Fig. 7** Development of the dilation wave for the high density fill at four different times. The *arrows* indicate the position of ‘arches’



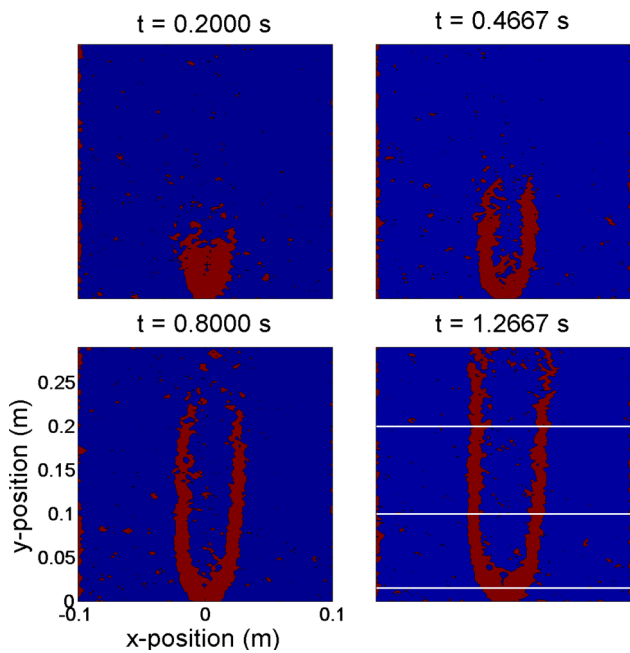
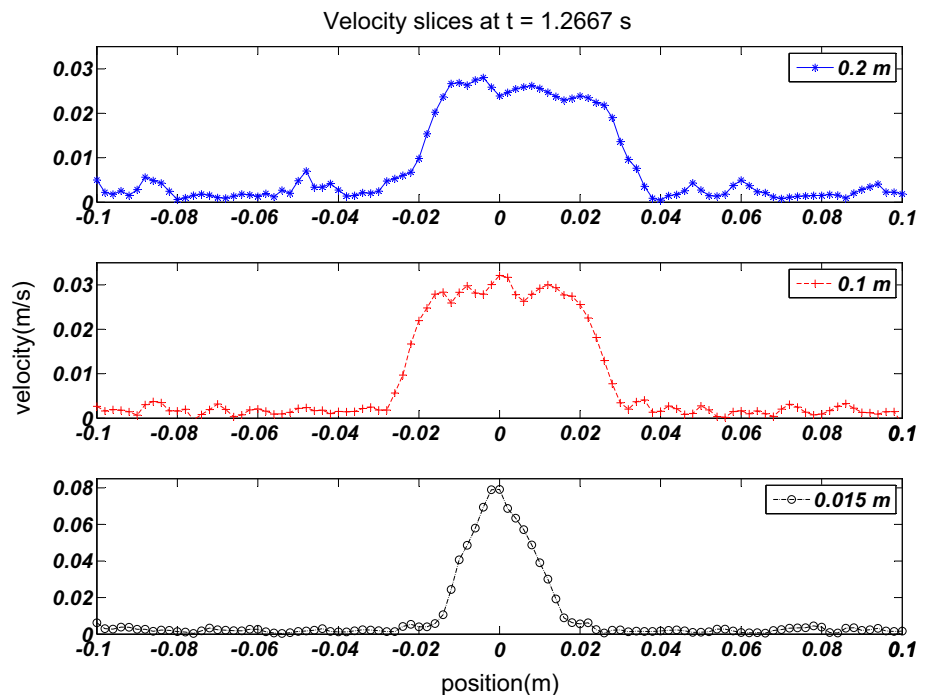


**Fig. 8** Regions of yielded (red) and unyielded (blue) material at four times. The white horizontal lines correspond to the locations of velocity slices of Fig. 9 (colour figure online)

arcs have formed, two more dilation bands appear which propagate from the edges of the arch upwards, then form a second arc. This process was repeated three times before the dilation wave reached the top of the domain. The material enclosed by the arcs appears to flow at a higher density than the material at the dilation lines. It visually appeared that this

enclosed material flowed in a plug-like manner, which suggests that the material has not yet reached yield. To explore this hypothesis we numerically calculate  $\|\dot{\gamma}\| = \sqrt{\frac{1}{2}\dot{\gamma}_{ij}\dot{\gamma}_{ij}}$ , the second invariant of the shear-rate tensor at of the flow at the times of Fig. 7. When the material is below yield it does not shear, hence the second invariant should be zero. In practice, however, the PIV process is inherently noisy and even stagnant material may (numerically) display non-zero shear. To overcome this issue we calculated  $\|\dot{\gamma}\|$  in the regions in which we knew the material to be stagnant and calculated the average shear at yield,  $Y_{ave}$ , as well as the standard deviation  $\sigma_{Yield}$ . These values were used to create a threshold,  $Y_{ave} + 3\sigma_{Yield}$ , below which we consider the granular material unyielded, above which the material should shear. Figure 8 displays the results of this thresholding. The red region encircling the blue region are the corresponding shear zones of Fig. 7. In this zone the stress that the material experiences exceeds yield, and the material shears. Between these shear zones the material appears to be below yield, and flows in a plug-like fashion. Outside of these zones the material is stagnant and has not reached yield, hence is also blue. As a second visualisation of this yielding, we take three slices of the last image in Fig. 8 (the locations of which are marked with white horizontal lines in Fig. 8) and plot the velocity magnitude there. These slices were taken at 0.02, 0.1, and 0.2 m above the orifice and are displayed in Fig. 9. From Fig. 8 it is apparent that near the orifice, at 0.02 m, the material is yielded and shears. The corresponding velocity slice in Fig. 9 shows a Gaussian-type velocity curve, commonly seen in granular silo flows. However, the slices taken at 0.1

**Fig. 9** Horizontal slices of the velocity magnitude at locations above the orifice at  $t = 1.2667$  s. Near the orifice the velocity has a Gaussian-like shape and shears, but far away from the orifice there is a flattening of the velocity peak, indicating a plug-like flow



and 0.2 m cross the two shear planes with unyielded material between. The effect of this is apparent in the plots of Fig. 9. The nicely peaked Gaussian curve is now replaced with a relatively flat (plug-like) velocity in the middle zone between the shear planes.

## 4 Conclusions and Discussion

We have studied the development of granular dilation waves generated during the transition from solid to liquid-like flow states. An X-ray technique and high-speed video analysis were used to visualise the dilation waves. In Sect. 3.1 the volumetric flow rate was shown to develop very rapidly regardless of the initial packing density of the bed. This was expected, since the flow rate from the orifice is determined locally by the so-called free fall arch [4, 34] rather than by the dynamics of flow higher in the silo. One consequence of this constant flow rate was observed in Sect. 3.3 where it was noted that the width of the flowing zone took a significant time to develop. The width of this zone controlled the velocities in the system, since, to keep a constant flow rate, the vertical velocities were necessarily larger when the flowing zone was narrow. For the high density fill, it was noted that the change in density during flow initiation was visible on the X-ray images, and these matched well with the flow initiation position obtained from PIV. However, changes in density during flow initiation were not visible for the low density fill, indicating that the filling bulk density of  $800 \pm 10 \text{ kg/m}^3$  was close to the flowing density of the grains. We noted that the dilation wave for the low density fill propagated significantly faster than for the high density fill, and the vertical speed of the dilation wave was measured in Sect. 3.4, using the high speed images. The speed of the dilation wave front was found to be highly dependent on the initial packing density. Differences of an order of magnitude were found, with vertical wave speed increasing significantly with decreasing solids fraction. This behaviour was captured in a simple mathematical model in Sect. 3.6. The model was derived by considering conservation of mass principles. It was shown to capture the measured dilation wave speeds, and was very sensitive to the difference between initial packing and flowing density. In all cases studied here, the dilation wave propagated faster than the granular flow velocity in the system. In Sect. 3.6 we examined the structure of the dilation wave by calculating the second invariant of the shear rate tensor. It was shown that during flow initiation there are symmetric thin shear “fault” zones where the granular material begins to flow. Between these zones is a plug zone which flows like a solid, and outside these zones the flow is stagnant. Such observations are important in the analysis of natural hazards such as avalanches [10]. The packing density of debris or snow can vary significantly depending on the consolidation

process which will lead to differences in dilation wave behaviour. We hypothesize that such dilation speed differences will lead to different run-out dynamics once an avalanche is triggered. The presence of dilation waves has been reported in some DEM studies [2]. It is of interest to see if DEM simulations (or, indeed, other granular flow models) can replicate the variable dilation wave speed with differing initial bulk density. Discrete models seem best suited to capture such phenomena as they are able to account for changes in the volume fraction (dilation) [30]. Finally, we have shown that the volumetric flow rate develops much more rapidly than the dilation wave. The system does not reach a true steady state until the dilation wave has propagated throughout the silo,  $\approx 40 \text{ s}$ . This result may have implications for common measurements of granular systems such as the residence time distribution or segregation [8, 9, 14, 15]. Such experiments will need to account for the transition to steady state. Such assumptions must be tested experimentally, and the authors are pursuing such a measurement. Mathematical modelling of transient granular flow, and in particular of dilation wave propagation is a necessary future step. It is hoped that recent advances in granular rheology [12, 17, 22, 29] can be extended to the transient regime, although it is likely that a two-phase formulation will be necessary to account for dilatancy effects [26]. We also noted that regions of flow may be shearing, while others may flow in a plug-like fashion due to not having exceeded a yield stress. Simple mathematical models, such as those based upon Mohr-Coulomb laws, may not capture such yield effects, and there is a need to further advance mathematical models of dense granular flows to account for this.

**Acknowledgements** The authors would like to acknowledge the Massey University Research Fund (MURF) for funding. We also thank Bronwen Comrie-Evans and John Edwards for the use of laboratory space, and Diane Orange for helpful discussions and access to the X-ray facilities. Finally, we thank the reviewers of this manuscript for their excellent suggestions for improvement during the first review of the manuscript.

### Compliance with ethical standards

**Conflict of interest** The authors acknowledge the Massey University research fund for providing funding for this project. The authors have no conflicts of interest to declare.

## References

1. Ancy, C., Coussot, P., Evesque, P.: A theoretical framework for granular suspensions in a steady simple shear flow. *J. Rheol.* **43**(6), 1673–1699 (1999)
2. Balevičius, R., Kačianauskas, R., Mróz, Z., Sielamowicz, I.: Analysis and dem simulation of granular material flow patterns in hopper models of different shapes. *Adv. Powder Technol.* **22**(2), 226–235 (2011)

3. Baxter, G.W., Behringer, R., Fagert, T., Johnson, G.A.: Pattern formation in flowing sand. *Phys. Rev. Lett.* **62**(24), 2825–2828 (1989)
4. Brown, R., Richards, J.C.: *Principles of Powder Mechanics*. Pergamon Press, Oxford (1970)
5. Delaplane, J.W.: Forces acting in flowing beds of solids. *AIChE J.* **2**(1), 127–138 (1956)
6. Faqih, A., Chaudhuri, B., Muzzio, F.J., Tomassone, M.S., Alexander, A., Hammond, S.: Flow-induced dilation of cohesive granular materials. *AIChE J.* **52**(12), 4124–4132 (2006)
7. Fickie, K.E., Mehrabi, R., Jackson, R.: Density variations in a granular material flowing from a wedge-shaped hopper. *AIChE J.* **35**(5), 853–855 (1989)
8. Fullard, L., Davies, C.: A brief investigation into ejection times from a conical mass flow hopper-coulomb and conical model difference. In: *POWDERS AND GRAINS 2013: Proceedings of the 7th International Conference on Micromechanics of Granular Media*, vol. 1542, pp. 1254–1257. AIP Publishing (2013)
9. Fullard, L.A., Davies, C.E., Wake, G.C.: Modelling powder mixing in mass flow discharge: a kinematic approach. *Adv. Powder Technol.* **24**(2), 499–506 (2013)
10. Gravish, N., Goldman, D.I.: Effect of volume fraction on granular avalanche dynamics. *Phys. Rev. E* **90**(3), 032202 (2014)
11. Haw, M.: Jamming, two-fluid behavior, and self-filtration in concentrated particulate suspensions. *Phys. Rev. Lett.* **92**(18), 185506 (2004)
12. Henann, D.L., Kamrin, K.: A predictive, size-dependent continuum model for dense granular flows. *Proc. Natl. Acad. Sci.* **110**(17), 6730–6735 (2013)
13. Hunt, M., Zenit, R., Campbell, C., Brennen, C.: Revisiting the 1954 suspension experiments of RA Bagnold. *J. Fluid Mech.* **452**, 1–24 (2002)
14. Johanson, K.: Predicting cone-in-cone blender efficiencies from key material properties. *Powder Technol.* **170**(3), 109–124 (2006)
15. Johanson, K., Eckert, C., Ghose, D., Djomlija, M., Hubert, M.: Quantitative measurement of particle segregation mechanisms. *Powder Technol.* **159**(1), 1–12 (2005)
16. Jyotsna, R., Kesava Rao, K.: A frictional-kinetic model for the flow of granular materials through a wedge-shaped hopper. *J. Fluid Mech.* **346**, 239–270 (1997)
17. Kamrin, K., Bazant, M.Z.: Stochastic flow rule for granular materials. *Phys. Rev. E* **75**(4), 041301 (2007)
18. Kulkarni, S.D., Metzger, B., Morris, J.F.: Particle-pressure-induced self-filtration in concentrated suspensions. *Phys. Rev. E* **82**(1), 010402 (2010)
19. Lube, G., Huppert, H.E., Sparks, R.S.J., Freundt, A.: Static and flowing regions in granular collapses down channels. *Phys. Fluids* **19**(4), 043301 (2007)
20. Mastbergen, D.R., Van Den Berg, J.H.: Breaching in fine sands and the generation of sustained turbidity currents in submarine canyons. *Sedimentology* **50**(4), 625–637 (2003)
21. Michalowski, R.: Flow of granular material through a plane hopper. *Powder Technol.* **39**(1), 29–40 (1984)
22. MiDi, GdR.: On dense granular flows. *Eur. Phys. J. E* **14**(4), 341–365 (2004)
23. Muite, B.K., Quinn, S.F., Sundaresan, S., Rao, K.K.: Silo music and silo quake: granular flow-induced vibration. *Powder Technol.* **145**(3), 190–202 (2004)
24. Nedderman, R.M.: *Statics and Kinematics of Granular Materials*. Cambridge University Press, Cambridge (2005)
25. Pailha, M., Nicolas, M., Pouliquen, O.: Initiation of underwater granular avalanches: influence of the initial volume fraction. *Phys. Fluids* **20**(11), 111701 (2008)
26. Pailha, M., Pouliquen, O.: A two-phase flow description of the initiation of underwater granular avalanches. *J. Fluid Mech.* **633**, 115–135 (2009)
27. Sielamowicz, I., Błoński, S., Kowalewski, T.A.: Digital particle image velocimetry (dpiv) technique in measurements of granular material flows, part 2 of 3-converging hoppers. *Chem. Eng. Sci.* **61**(16), 5307–5317 (2006)
28. Sigmund, W., El-Shall, H., Shah, D.O., Moudgil, B.M.: *Particulate Systems in Nano-and Biotechnologies*. CRC Press, London (2008)
29. Staron, L., Lagrée, P.Y., Popinet, S.: Continuum simulation of the discharge of the granular silo. *Eur. Phys. J. E* **37**(1), 1–12 (2014)
30. Taberlet, N., Richard, P., Jenkins, J., Delannay, R.: Density inversion in rapid granular flows: the supported regime. *Eur. Phys. J. E* **22**(1), 17–24 (2007)
31. Thielicke, W.: *The flapping flight of birds-analysis and application*. Ph.D. thesis, Rijksuniversiteit Groningen (2014)
32. Thielicke, W., Stamhuis, E.J.: Pivlab-towards user-friendly, affordable and accurate digital particle image velocimetry in matlab. *J. Open Res. Softw.* **2**(1), e30 (2014)
33. Thompson, P.A., Grest, G.S.: Granular flow: friction and the dilatancy transition. *Phys. Rev. Lett.* **67**(13), 1751 (1991)
34. Thorpe, R.: An experimental clue to the importance of dilation in determining the flow rate of a granular material from a hopper or bin. *Chem. Eng. Sci.* **47**(17), 4295–4303 (1992)
35. Vivanco, F., Melo, F., Fuentes, C.: Granular flow models and dilation front propagation applied to underground mining. *Int. J. Bifurc. Chaos* **19**(10), 3533–3539 (2009)
36. Weir, G.J.: A mathematical model for dilating, non-cohesive granular flows in steep-walled hoppers. *Chem. Eng. Sci.* **59**(1), 149–161 (2004)
37. Yaras, P., Kalyon, D., Yilmazer, U.: Flow instabilities in capillary flow of concentrated suspensions. *Rheol. Acta* **33**(1), 48–59 (1994)
38. Yukawa, S., Kikuchi, M.: Density fluctuations in traffic flow. *J. Phys. Soc. Jpn.* **65**(4), 916–919 (1996)